International Symposium
On Turbulence and Shear Flow
Phenomena (TSFP-9)
June 30 - July 3, 2015 Melbourne, Australia

COMPRESSIBILITY EFFECTS ON TURBULENT SHEAR FLOWS

Neil D. Sandham
Aerodynamics and Flight Mechanics Group
Faculty of Engineering and the Environment, University of Southampton
Southampton SO17 1BJ, UK
n.sandham@soton.ac.uk

ABSTRACT

Compressibility effects are present in many practical turbulent flows, ranging from shock-wave/boundary-layer interactions on the wings of aircraft operating in the transonic flight regime to supersonic and hypersonic engine intake flows. Besides shock wave interactions, compressible flows have additional dilatational effects and, due to the finite sound speed, pressure fluctuations are localized and modified relative to incompressible turbulent flows. Such changes can be highly significant, for example the growth rates of mixing layers and turbulent spots are reduced by factors of more than three at high Mach number. In this paper we review some of the basic effects of compressibility on canonical turbulent flows and attempt to rationalise the different effects of Mach number in different flows using a flow instability concept. We then turn our attention to a fully three-dimensional problem of shock-wave/boundary-layer interaction in a closed duct, considering direct effects of shock waves, due to their penetration into the outer part of the boundary layer, as well as indirect effects due to the high convective Mach number of the shock-induced separation zone. It is noted in particular how shock-induced turning of the detached shear layer results in strong localized damping of turbulence kinetic energy.

INTRODUCTION

While shock-wave interactions with turbulent boundary layers were known since basic experiments conducted in the 1940s (Dolling, 2001), it became apparent in subsequent work that more subtle effects of compressibility were also present, for example in the experimental data on mixing layers collated by Birch & Eggers (1973) that showed a large reduction in growth rate as the Mach number increased. Indeed this was one of the motivations for the Brown & Roshko (1974) work on mixing layers that, besides stimulating work on organised structures in turbulence, also demonstrated that the reductions in growth rate could not be attributed solely to the effects of variable density. However other flows, such as attached turbulent boundary layers, did not show strong effects of compressibility, with Morkovin's hypothesis (Bradshaw, 1977) of weak compressibility applying up to Mach 5. Some of the apparent contradictions have been resolved in subsequent research, while some aspects, including turbulence and sub-grid modelling for compressible flows, are unresolved. A number of reviews of compressible turbulence and shock-wave/boundary-layer interaction (SWBLI) have been published over the last decade, including Smits & Dussauge (2006), Gatski & Bonnet (2009), Babinsky & Harvey (2011) and Clemens & Narayanaswamy (2014).

In this contribution we will first review the main canonical flow problems and then discuss flow stability arguments that, in connection to turbulence production at the largest eddy scales, can help to explain some of the differences seen between different flows such as the mixing layer and wall boundary layer. We then consider a more practical example of SWBLI in a 3D duct flow, where multiple effects are present but additional physics is still observed in the form of streamline curvature effects.

CANONICAL FLOWS

Mixing layers

The most striking effect of compressibility on turbulence is the reduction in growth rate of the compressible turbulent mixing layer. Experiments by Papamoschou & Roshko (1988) showed how a convective Mach number and a suitable normalisation of mixing layer growth rate with its incompressible value could collapse data over a wide range of Mach number and density ratios. For free-streams with equal ratio of specific heats, the convective Mach number is given by $M_c = (U_1 - U_2)/(a_1 + a_2)$, where U is the velocity and a the sound speed with subscripts 1 and 2 denoting the fast and slow speed streams respectively. M_c can be interpreted as the free-stream Mach number seen by an eddy convecting downstream at a velocity of $U_c = (a_2 U_1 + a_1 U_2)/(a_1 + a_2)$. The most comprehensive attempt to collapse the experimental data is in Slessor *et al.* (1998), who used a slightly modified version of the convective Mach number to get a best fit. For two parallel streams with equal ratio of specific heats and equal free stream temperatures the resulting curve is shown in figure 1, in the form of a plot of the relative growth rate Φ (the mixing layer spreading rate under compressible flow conditions, divided by the spreading rate in incompressible flow for the same velocity and density ratio) against the convective Mach number M_c. The growth rate of the turbulent wedge is seen to be reduced by almost a factor of three as the convective Mach number is raised to 1.0. Despite a considerable spread in the experimental data, the convective Mach number concept appears to be well supported by experimental data. Figure 1 also shows a curve from linear stability theory (LST), showing the effect of Mach number on the temporal growth rate (taking the maximum over all streamwise and spanwise wavenumber combinations). We shall return later to the observation that the linear theory follows the Slessor *et al.* (1998) empirical fit quite closely

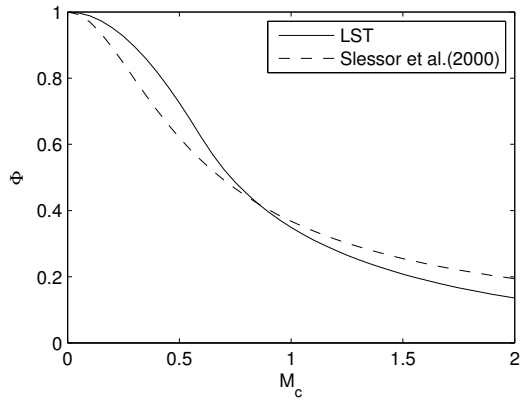

Figure 1. Relative growth rate Φ as a function of convective Mach number M_c, showing results from linear stability theory (LST) compared with the empirical fit to experimental data from Slessor *et al.* (1998).

(within the experimental scatter).

An explanation for the reduction in growth rate has been sought from the Reynolds stress transport equations. Early suspicions fell on the additional terms in these equations that are not present in incompressible flows. However, Vreman *et al.* (1996) showed that the dilatation dissipation and pressure dilatation terms remained small even as the growth rate reduced significantly due to compressibility. It was shown instead how the growth rate falls in proportion to the production and that this in turn was caused by reductions in pressure strain terms in the Reynolds stress equations. Thereafter, explanations differ as to the root cause. Vreman *et al.* (1996) considered a model compressible vortex, showing how pressure fluctuations naturally reduced in compressible flows, and how a model based on this idea could predict the growth rate reduction, whereas Pantano & Sarkar (2002) considered the effect of reduced communication due to the finite sound speed. However to the author's best knowledge neither the reduced communication idea nor the reduced pressure fluctuations have been used in practical turbulence models to date.

Boundary layers

It is well known that compressible wall boundary layers are mainly affected by density effects, rather than compressibility, for free stream Mach numbers $M_\infty \leq 5$ (Bradshaw, 1977). The standard way to scale density effects out of the mean profile is with the Van Driest transformation, given by

$$u^+_{\mathrm{VD}} = \int_0^{u^+} \left(\frac{\rho}{\rho_w}\right)^{1/2} du^+ \qquad (1)$$

The transformed profiles have been observed to provide a useful (though not exact) collapse of high speed boundary layer profiles back onto incompressible cases, as shown for example in Duan & Martin (2011). The transform has also been used to extend tubulence inflow generation methods to fully compressible flow, for example in Touber & Sandham (2009).

Early progress on understanding the effect of compressibility on boundary layer turbulence was reviewed by Bradshaw (1977). He expressed the findings as a number of hypotheses and analogies between energy and momentum transport. Morkovin's hypothesis covers an expectation that the turbulence shear stress and streamwise normal stress are not strongly dependent on Mach number, whereas the strong Reynolds analogy uses a linearisation of the governing equation to connect thermodynamic and velocity fluctuations. Evidence for applicability or otherwise of these relations is provided by DNS studies, including Maeder *et al.* (2001). In particular, Huang *et al.* (1995) and Duan & Martin (2011) show how the analogies can be adapted for high Mach number and high enthalpy flows to provide reasonable representations of the turbulence.

Other insights have helped to understand the different effects of Mach number on different flows. In particular the gradient Mach number M_g was exploited by Sarkar (1995) to compare mixing layers with boundary layers, since it was found that for equivalent flow Mach numbers the gradient Mach number was substantially higher in mixing layers. This study also first identified the role of compressibility in modifying the production rate of turbulence.

The state of turbulence modelling for compressible flows is discussed in Wilcox (2006), which despite being ten years old still represents the state of the art. Wilcox describes a number of fixes to low-speed models to account for both the rapid change of mixing layer growth rate with Mach number and the relative insensitivity of the boundary layer to Mach number. These fixes are purely empirical and the lack of progress in modelling has been a disappointment. One approach was based on dilatation dissipation, for example in Sarkar *et al.* (1991), which considered the additional dissipation due to eddy shocklets. However, the modelling did not develop on a more physically-based pathway once the origin of the growth rate was found to reside in pressure-strain correlation rather than explicit compressibility terms (Vreman *et al.*, 1996).

Large-eddy simulation is also problematic for compressible flow due to the large number of sub-grid terms that may need to be modelled, as discussed in Garneir *et al.* (2009). Vreman (1995) recognised the problem and overcame it to some extent by proposing dynamic models that do not require any particular physical insight into the nature of the various terms. The issue of compressibility is probably not so serious for LES as for RANS, since most of the strong compressibility is expected to reside in the larger scales. Nevertheless, shocks and eddy shocklets have spectral content at the smallest scales and this is not generally taken into account in the models. An additional problem in DNS and LES is that the dissipation introduced into numerical schemes to allow the capturing of shock waves is also likely to over-damp turbulence, unless particular attention is paid to the schemes and to the use of limiters to restrict the dissipation to the immediate vicinity of shocks.

Turbulent spots

Given the relative insensitivity of zero pressure gradient boundary layers to the free-stream Mach number, it is surprising that lateral growth rate of turbulent spots (regions of a turbulence within an otherwise laminar boundary layer) is strongly affected by compressibility. A collection of experimental data by Fischer (1972) shows a reduction in spreading angle by a factor of three at $M_\infty = 5$, compared with incompressible flow (where the spreading half angle is about 10°). In the years since the experimental data was published, it has become possible to carry out numerical simulations of some of the cases, with examples reported in

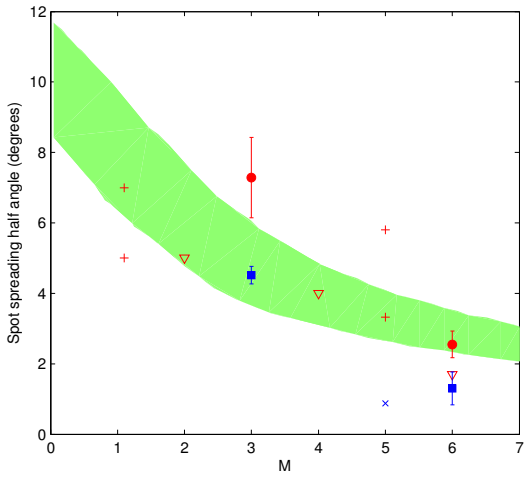

Figure 2. Variation of the spreading angle of the half-width of turbulent spots as a function of free-stream Mach number (Redford *et al.*, 2012). The shaded area represents the spread of the experimental data from Fischer (1972), while the symbols show DNS results from Jocksch & Kleiser (2008) (+), Krishnan & Sandham (2006) (open symbols) and Redford *et al.* (2012) (filled symbols, red for hot wall conditions and blue for cold-wall conditions).

Krishnan & Sandham (2006) and Jocksch & Kleiser (2008). It is interesting to note that there are varying definitions of spot width and numerical simulations show similar scatter to the experiments, as shown in figure 2. Further calculations by Redford *et al.* (2012) show the expected reductions in growth rate and also show how the wall thermal condition is of lesser importance than the Mach number. Cases with cold walls (wall temperature equal to the free stream temperature spread more slowly than spots in flows where the walls are at the adiabatic temperature, but only by 20-30%, whereas the spreading rate at $M_\infty = 6$ was already reduced by a factor of four compared to incompressible flow.

Why should compressibility be so important to the spreading of turbulent spots, but play only a minor role in the fully developed turbulent boundary layer? To explain this, attention has focused on the wing-tip region where the boundary between turbulent and laminar flow provides a strong lateral velocity gradient that can drive the spot growth. Gad-El-Hak *et al.* (1981) noted that the turbulence can spread by two mechanisms, either by mean convection outwards from the spot centre, or by destabilisation of the surrounding boundary layer. Once fluid has become turbulent it can be thought of as being convected at typical speeds associated with structures within the turbulent flow. Structures towards the edge of the boundary convect at near the free stream speed, while those closest to the wall (the near wall streaks and buffer layer structures) convect at speeds of 40-50% of the free stream, dependent on Reynolds number. This leads to a natural streamwise spreading of the newly-turbulent flow that, together with the lateral spreading, gives the classical arrow-head structure of spots. This structure is changed by compressibility, with examples of turbulent spots shown in Redford *et al.* (2012). Additional structures related to the second (Mack) modes of instability are also observed underneath the spots (Krishnan & Sandham, 2006). With respect to the growth mechanism that was affected by compressibility, Redford *et al.* (2012) showed how it was the destabilisation of the surrounding boundary layer (Gad-El-Hak's second mechanism) that was affected by Mach number, with a much slower rate of generation of new structures at the Mach 6 compared to Mach 3 in their simulations. The relevance of an instability/destabilisation mechanism for spot growth is something that we will follow up later.

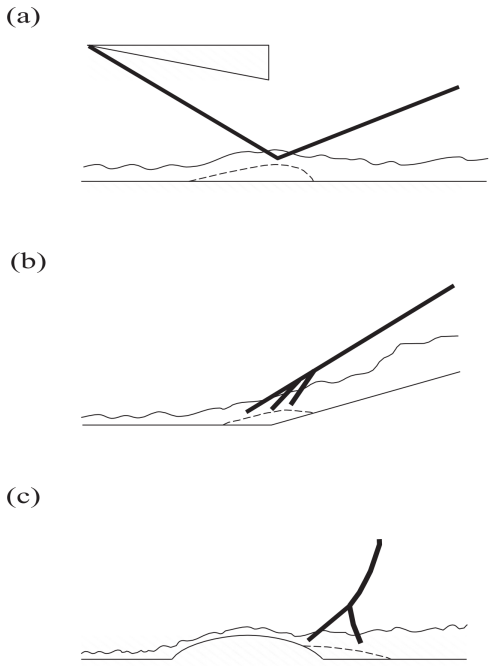

Figure 3. Three different types of shock-wave/boundary later interaction problems: (a) shock impingement, (b) supersonic ramp flow, (c) transonic flow over a bump (Lawal, 2002).

Shock/turbulence interaction

A simple model problem consists of isotropic turbulence passing through a normal shock, for which direct numerical simulations (DNS) and a linearised theory are possible. Linearised interaction analysis (LIA) is derived from the Euler equations. The oncoming turbulence can be decomposed into vortical, acoustic and entropy modes, which can in principle interact with each other according to the mechanisms given in Chu & Kovásznay (1958). To study shock/turbulence interactions, each of the linear modes can be interacted separately with a normal shock wave. Results from comparisons between DNS and linear theory are reported in e.g. Mahesh *et al.* (1997), who looked in particular at the variations in turbulence associated with an entropy wave passing through a normal shock. Turbulence kinetic energy and temperature fluctuations are amplified across the shock, with the streamwise normal stress being most affected. Whereas generally a good qualitative agreement has been found between DNS and theory, recent work by Larsson *et al.* (2013) has identified some important differences. The post-shock anisotropy of vorticity was found to be of small practical importance due to a rapid return to isotropy at higher Reynolds numbers. Additionally different flow regimes in which the shock wave became wrinkled and broken were identified.

Shock-wave/boundary-layer interaction

When a shock wave interacts with a boundary layer the subsequent interaction can be weak, where the boundary layer is thickened by the adverse pressure gradient imposed by the shock, or strong, where there is a shock-induced flow separation. This category of canonical flow can be further subdivided as shown in figure 3 into: (a) an oblique shock impinging onto a boundary layer on a flat plate, (b) an interaction initiated by a ramp and (c) a transonic interaction in flow over a bump. The latter case is different, since the flow upstream and downstream is subsonic. However all three cases share important flow physics, including separation, with a shock wave developing from the coalescence of compression waves from the separation region, and a similar phenomenon leading to a reattachment shock, with a closed separation bubble forming in each case. The bump flow forms a classical λ-shock pattern, where the two shocks near the wall (forming the front and rear feet) meet at a triple point. Above this region a near-normal shock marks the end of the supersonic flow region. The oblique shock and ramp cases have similar physics, as shown for small disturbance cases by Pagella *et al.* (2004). However there are important potential differences, with many observations of streamwise structures attributed to Görtler instability due to the destabilising curvature near the reattachment point. There are also curvature effects in the oblique shock case, as we shall see later, and it is important to note that the flow over the top of the bubble in this case also experiences an expansion fan and the bubble in this case is triangular in shape, with the apex at the point where the shock impinges and reflects as an expansion wave.

All three cases show similarities in the difficulty of the turbulence modelling and in the occurrence of large amplitude low-frequency oscillations. The former problem is well known. Reynolds-averaged Navier-Stokes (RANS) methods give results of only qualitative accuracy, as for example shown by Doerffer *et al.* (2010). One might think that the unsteadiness can be captured in unsteady RANS (URANS), but this method only gives steady results, as does detached eddy simulation (DES). Better agreement with experiment can only be obtained with such methods by introducing additional unsteadiness, as shown by Garnier (2009), but this requires the specification of disturbances, the precise form of which is not known a priori. This is an ongoing research topic, as is the embedding of higher fidelity methods within RANS, URANS and DES. The lowest form of modelling that has been proven to work for SWBLI problems is LES, and only then with wall-resolved LES, by which we mean LES that resolves the sublayer, with grid grid counts smaller than DNS by only a factor of 20-30 and with care taken particularly to resolve the wall-normal direction close to what would be needed for DNS. The first application of LES to the oblique SWBLI problem was by Garnier *et al.* (2002). Such simulations can show excellent agreement with experiment, as for example shown in figure 4 where results from Touber & Sandham (2009) are compared with experiments carried out in Marseille by Dupont *et al.* (2006) and Piponniau *et al.* (2009), although we should bear in mind the sensitivity of the experimental flow to upstream conditions and sidewall effects, and of the LES to the spanwise domain size. Nevertheless, it is clear that LES captures the correct bubble physics. Furthermore, LES is the only feasible way to obtain sufficiently long time series to be able to study the other interesting feature of shock-induced separated flow, namely the low-

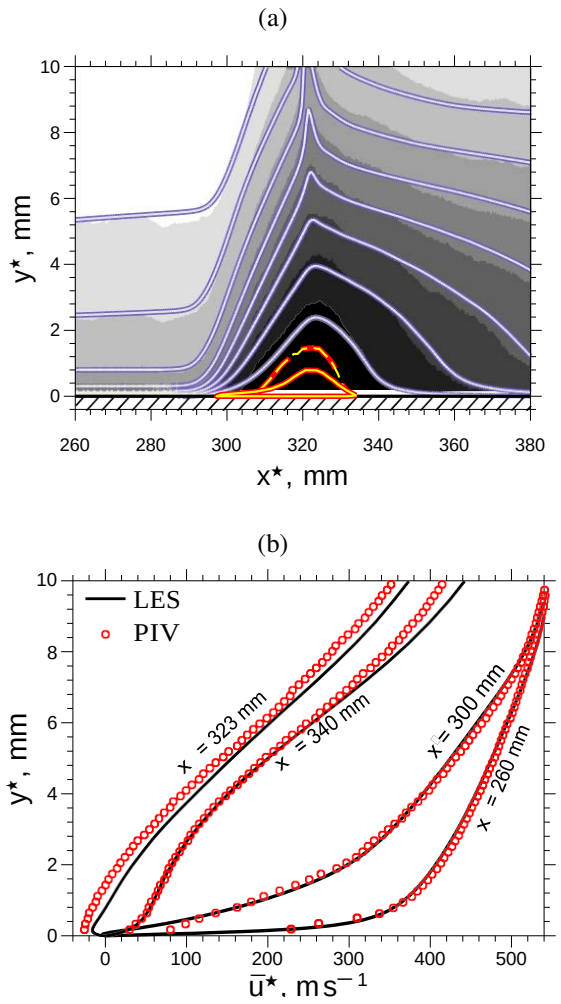

Figure 4. Comparison of LES with experiment showing (a) contours of mean streamwise velocity, comparing PIV (shaded) with LES (contour lines), with the orange lines (dashed for the experiment) showing the zero velocity contour, and (b) velocity profiles at several streamwise locations (Touber, 2010).

frequency unsteadiness.

There are a number of competing explanations of the occurrence of low-frequency oscillations in SWBLI problems, and it is only very recently that a resolution appears to be possible. Figure 5 shows a weighted (pre-multiplied with frequency) power spectrum of wall pressure fluctuations under the base of the reflected shock. The figure shows a good agreement between the experimental measurements (Dupont *et al.*, 2006) and LES. The LES shows two peaks, one at Strouhal number of $St = 0.03$ and the other (not resolved in the experiment) corresponding to boundary layer turbulence. Alternative explanations for the low-frequency peak include upstream boundary-layer disturbances, global modes, acoustic feedback mechanisms within the bubble and bubble 'breathing'. We will not recap all the arguments here; they are readily available in the literature, for example in Ganapathisubramani *et al.* (2007), Robinet (2007) Pirozzoli & Grasso (2006) and Piponniau *et al.* (2009). Each study is in some sense correct in that the physical phenomena are reproducible, but there is generally a lack of testable predictions from the various approaches. A resolution appears possible when we consider two recent developments.

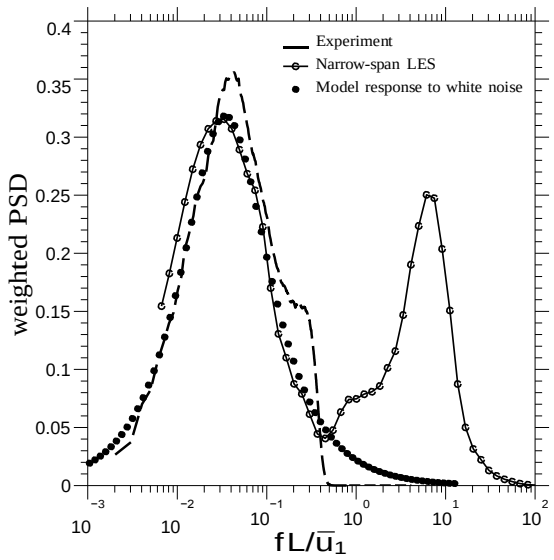

Figure 5. Weighted power spectral density of wall pressure fluctuations as a function of normalised frequency, comparing experiment (dashed line), LES (line with open symbols and the model (filled symbols), from Touber (2010).

Firstly Touber & Sandham (2011) showed how an analysis based on the (wall-normal) integrated Navier-Stokes equations, using LES data to neglect terms with lower order of magnitude, could provide a simplified model in the form of a first order ordinary differential equation, with stochastic forcing provided by the boundary layer skin friction fluctuations (either upstream or downstream of separation). Remarkably, this results in exactly the same spectrum as was postulated empirically by Plotkin (1975). The prediction of this type of model is shown with filled symbols on figure 5, with excellent agreement between the model and both LES and experiment. The analysis only requires the flow near the separation to be modelled, suggesting that bubble feedback dynamics (recirculation or acoustic in origin) does not need to be included. Another useful way of looking at the problem is provided by the recent work of Sartor (2014), who used a resolvent mode analysis to look at the global response of a transonic bump flow problem (the Delery bump). This linearised analysis considers forcing in the problem formulation and the resulting singular value decomposition provides information about the flow response to forcing and about the forcing that gives the largest gain. Sartor did not find any globally unstable modes and showed how the response problem correctly picked out the dynamics of shock and shear layer interactions. The optimal forcing showed both upstream and downstream contributions, whereas in practical applications it would be modified by the disturbance environment. For example, it is known that the low-frequency response occurs even in the absence of upstream coherent disturbances (Touber & Sandham, 2009), or indeed any disturbances at all in the laminar case (Sansica *et al.*, 2014). Our current best explanation is therefore that the low-frequency unsteadiness is the linear response of the separating flow to background noise, with the shock acting as a low-pass filter of disturbances that can come from upstream or downstream. Near the separation

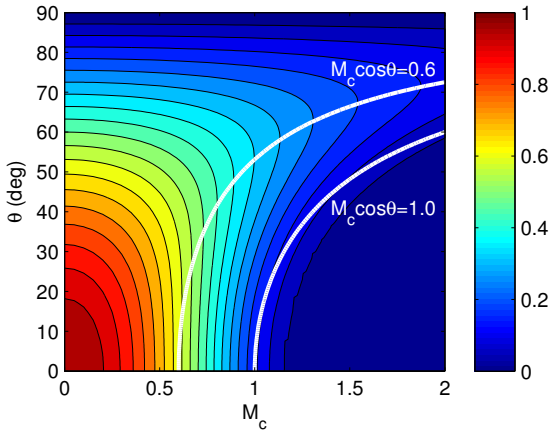

Figure 6. Contours of disturbance growth reduction factor Φ as a function of wave angle θ and convective Mach number M_c.

there is a high mean streamwise pressure gradient, hence the amplitude of the wall pressure fluctuations at this point is high.

THE $\theta - M_c$ STABILITY MAP

There have been a number of studies that make a connection between local stability analysis and turbulent free shear layer growth rates, for example Monkewitz & Huerre (1982). In particular the spatial growth rate of small amplitude disturbances seems to be directly proportional to the growth rate of a turbulent mixing layer. The rationale for this, that the growth and decay of long-wavelength modes (more than ten times the mixing layer vorticity thickness) controls the production of turbulence at large scales, was tested experimentally by Gaster *et al.* (1985), who showed that upstream forcing of instability waves could be quantitatively compared to the downstream behaviour of large structures in mixing layers. This was elaborated by Morris *et al.* (1990), who showed how the proportionality between linear spatial growth rate and mixing layer growth rate could be derived from a simplified model. Further evidence for the continued importance of linear modes has emerged in the study of jet noise; for example Suzuki & Colonius (2006) measured disturbances in the potential flow just outside a circular jet, with clear detection of the linear eigenmodes of the jet shear layer.

For compressible flows the relation between mixing layer growth rate and spatial stability theory was recognised by Ragab & Wu (1989) and Sandham & Reynolds (1990). In particular it was shown how the effect of velocity ratio, density ratio and Mach number on mixing layer growth rate could all be predicted by the linear theory. In this section we present the basic shear layer instability results in the form of a $\theta - M_c$ map, where θ is the wave angle and M_c is the convective Mach number, and we will attempt to find definitions of an effective M_c (different to the gradient Mach number M_g) for boundary layers and turbulent spots.

The basic $\theta - M_c$ plot is shown on figure 6. The vertical axis is the wave angle θ, which is equal to zero for spanwise wavefronts and 90° for streamwise wavefronts. The horizontal axis is the convective Mach number M_c. The contours on the stability map are of the growth reduction factor Φ, which is defined as the growth rate relative to the

largest growth rate of the same case (same velocity and density ratio) from incompressible flow. Φ is defined by taking the maximum growth rate over all streamwise wavenumbers. In Sandham & Reynolds (1990) it was shown that the spatial and temporal theories provide very similar results for Φ, so here we use the temporal approach for simplicity and only consider cases with equal density ratio. The plot includes only first mode disturbances, which are oblique at the higher Mach numbers. There are also radiating modes, but these are only weakly unstable and can be ignored in this context. The first stages of oblique-mode breakdown to turbulence were presented based on DNS by Sandham & Reynolds (1991).

A number of interesting results are clearly seen from figure 6. At $M_c = 0$ the most unstable mode is 2D (a consequence of Squires' theorem). This is not to say that only 2D modes are excited, however. An N-factor calculation in Sandham & Sandberg (2009) showed how structures could emerge from background spectra including different angles. Neither this approach, nor the DNS, gave perfectly spanwise structures, implying that other factors may have been active in the Brown & Roshko (1974) experiments that showed clear spanwise organisation. As M_c increases in figure 6 it can be seen that for $M_c > 0.6$ oblique modes are the most unstable waves. The peak growth rate follows a line $M_c \cos\theta = 0.6$ (Sandham & Reynolds, 1990). The variation of Φ, taking the maximum over θ for each M_c was shown on figure 1 as the LST result. This curve matches the observed decrease in shear layer growth rate observed experimentally, almost as well as the empirical fit to the data. Finally we note that for $M_c \cos\theta > 1$ (the second contour shown on figure 6) there is no first mode growth. Thus, for any local shear layer that is evolving within a turbulent flow, a dead zone occurs, with no instability (up to a certain wave angle) to drive shear-layer roll-up. This is expected to modify the turbulence dynamics at any scale where a locally-defined convective Mach number exceeds one.

The stability plot, extends straightforwardly to other free shear layers such as jets and wake. However we will also attempt to show in the following paragraphs how it may potentially also be applied to boundary layers, particularly under the effect of adverse pressure gradients, and to turbulent spots, by a suitable redefinition of M_c.

We have already remarked that compressibility effects enter the turbulence problem by modifying the production term, i.e. at the scale of the largest local structures, or alternatively where the velocity fluctuations are largest. For the boundary layer there are three possible regions where compressibility effects might enter, namely the buffer layer (which is exposed to a large velocity gradient), the log layer, and the outer (wake) region. Although the buffer layer is in a region of high velocity gradients, it is also typically a region of high temperature and hence high sound speed. This is sufficient to reduce considerably the effective value of M_c, for example a Mach 5 boundary layer with a wall temperature equal to the adiabatic wall temperature, a buffer layer $\Delta U^+ = 6$ and an edge velocity of $U_e^+ = 25$ would have an effective Mach number of $M_c = 0.05 M_\infty$, based on $M_c = \Delta U/(2a_w)$ putting this well within the region relatively unaffected by compressibility according to figure 6. Nevertheless, there can still be some effects of compressibility such as the changes in the low speed streaks observed by Coleman *et al.* (1995). In the log layer we can make a simple estimation based on the idea of a mixing length $l = \kappa y$ (with κ the von Karman constant). Here the effective Mach number, for a boundary layer with $U_e^+ = 25$ is given by $M_c = 0.02 M_\infty$, for the worst case of sound speeds a_1 and a_2 equal to the free stream value (a_e). The outer layer is more interesting because the form of the mean velocity profile that adds onto the log law to get to the observed data is already in the form of a mixing layer (i.e. Coles' wake function). We can develop an effective Mach number using the wake parameter Π and the respective sound speeds at the wall (a_w) and in the freestream (a_∞) by

$$M_{c,\mathrm{bl}} = \frac{2\Pi}{\kappa} \frac{M_\infty}{U_e^+(1 + a_w/a_\infty)}. \tag{2}$$

For the previously mentioned adiabatic wall case of $M_\infty = 5$ we get $M_{c,\mathrm{bl}} = 0.16$ which is low enough to be consistent with Morkovin's hypothesis, but higher than the other regions of the boundary layer, suggesting that the outer region is most susceptible to compressibility effects.

With adverse pressure gradient boundary layers the wake magnitude Π grows, up to the point of separation where we have effectively a mixing layer, and (aside from the not insignificant effects of wall proximity on the flow instability) we would expect that broadly the effect of compressibility will follow that seen for mixing layers. Thus, the prediction is that for adverse pressure gradient boundary layers, effects of compressibility will be seen at lower and lower Mach numbers. Taking the threshold at $M_c = 0.3$ we see that this is reached for cold-wall conditions ($a_w = a_\infty$) at $M_\infty = 5.5$ for zero pressure gradient flow, reducing down to $M_\infty = 0.6$ for a boundary layer on the point of separation or reattachment. Thus compressibility may be a significant effect in many transonic flow involving separation. This is not particularly a new observation but equation (2) above seems to provide a rationale to look for compressibility effects in boundary-layer flows with adverse pressure gradients at moderate M_∞.

Finally in this section we consider the growth of turbulent spots and the surprising result that even in zero pressure gradient boundary layers the lateral growth rate is strongly compressible, showing a reduction by a factor of four in a boundary-layer at $M_\infty = 6$. The reasons for this strong reduction have not yet been fully explored. Redford *et al.* (2012) showed how compressibility mainly acted on the mechanism of destabilisation of the surrounding laminar boundary layer and, perhaps most relevant to the mechanisms considered here, observed roll-up of lateral jets emanating from the wing tips of the spot. The local instability problem is not amenable to analysis since the basic flow is 3D. The jets themselves are not fast enough to be subject to high compressibility effects. However a simple estimate of M_c for these jets relative to the freestream can be derived, by considering the jet location in the laminar boundary layer, as

$$M_{c,\mathrm{spot}} = M_\infty \frac{1 - U_j/U_\infty}{1 + a_j/a_\infty} \tag{3}$$

where U_j is the laminar boundary layer streamwise velocity (and a_j the sound speed) at the jet location and from Redford *et al.* (2012) $U_j \approx 0.45 U_\infty$. For a spot at $M_\infty = 5$ we obtain $M_{c,\mathrm{spot}} \approx 1.0$, with a predicted value of $\Phi = 0.35$, which compares reasonably well with the observed spot growth rate curve.

In this section we have attempted to extend the basic shear layer instability arguments from mixing layers to

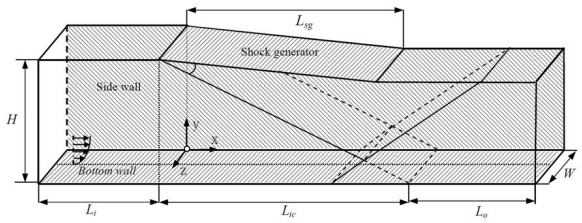

Figure 7. Schematic of SWBLI in a 3D duct with width W and height H, from Wang *et al.* (2015).

boundary layers with pressure gradients and to turbulent spots. These arguments are testable with more experiment and simulations of compressible boundary layers, particularly under conditions of adverse pressure gradient, and turbulent spots, where more understanding is needed of the physical mechanisms of spot growth.

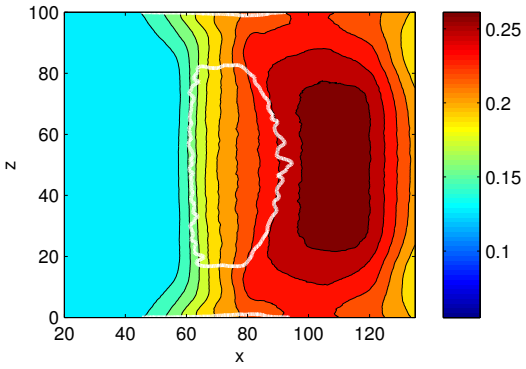

Figure 8. Mean pressure contours on the lower wall showing the pressure rise through the bubble and the end-wall effects. The white contours show the regions of reverse flow.

THREE-DIMENSIONAL SWBLI

In this final section we consider a fully 3D flow that in principle contains many of the phenomena reported in the previous sections. The test case is taken from Wang *et al.* (2015), which included both sidewalls in an $M_\infty = 2.7$ interaction of an oblique shock with a flat plate boundary layer. The $M_\infty = 2.7$ upstream boundary layer is not expected to experience strong compressibility effects until it enters the region of interaction with an oblique shock that is strong enough to separate the flow. Structures in the outer part of the boundary layer will experience shock/turbulence interaction and the separated shear flow will be affected by compressibility. In addition there are sidewall and corner interactions as well as a strong curvature of the shear layer due to the shock impingement.

Details of the simulations are given in Wang *et al.* (2015), with the basic set up reproduced in figure 7. After running the simulations all distances have been rescaled to units of mm in the corresponding experiment, whereas other quantities are shown in dimensionless form. The case is set up as a wall-resolved LES and a grid refinement study was run to show the sensitivity of the solution to the grid in each direction separately. The simulations shown here were run on a grid of $480 \times 416 \times 758$ points in the streamwise, normal and spanwise directions respectively. The inflow turbulent boundary is set using the same digital filter approach used by Touber (2010), with the inflow thickness adjusted to give a target Reynolds number of $Re_\theta = 4300$ based on the boundary layer at the shock impingement location, but in a case with no shock. The interaction is located sufficiently far downstream of the inflow to give the boundary layer enough time to relax to an equilibrium condition, measured by an acceptable comparison of the Van Driest scaled profile with incompressible flow data at the same Reynolds number. The cases were run for both sidewalls, since a test simulation with a symmetry plane in the spanwise direction gave unphysical results near that plane due to the constraints imposed of the turbulence by this boundary condition. The upper boundary condition is designed to mimic a shock generator in an experiment. Upstream of the shock generator a characteristic boundary condition was applied. On the shock generator a no-slip condition was set and then downstream the boundary condition was changed back to characteristic. Care was taken to ensure that the expansion wave emanating from the rear of the shock generator impacted on the lower test plate far enough downstream of the interaction not to affect the pressure and skin friction distributions within the interaction.

The shock generator (with angle 9°) generates an oblique shock. Depending on the aspect ratio W/H, where W is the width between the two sidewalls and H is the height of the leading edge of the shock generator above the plate, there are different types of interaction. In particular for a case with $W/H = 4$ it was shown that there is a region of genuinely span-independent mean flow near the centreline, with good agreement with a simulation run with spanwise periodic boundary conditions. This is because the sidewall-induced modifications to the impinging shock have not reached the centreline within the interaction region. In contrast, a case with $W/H = 1$ was shown to be completely 3D in the mean, as in Bermejo-Moreno *et al.* (2014). Here we consider the intermediate case $W/H = 2$, for which contours of surface pressure are shown on figure 8. The white contour line shows the reverse flow region, with the separation line seen to be more 2D than the reattachment line. Clear corner effects are observed, with the wall pressure rising earlier near the corners and with a small corner separation.

The nature of the interaction can be explained by tracing the effects back to the shock generator. The generated shock is sufficient to thicken, but not separate, the sidewall boundary layer. The pressure rise is thus smeared out and the start of the pressure rise precedes the shock location. Another interesting feature is that the shock does not penetrate the sidewall boundary layer down to the sonic line, but only down to a swept sonic condition. Wang *et al.* (2015) defined a penetration Mach number by $M_p = M_\infty \cos\beta$, where β is the oblique shock angle, and showed that this matched the actual penetration Mach number, observed as 2.2 in the simulations. Thus only the very outermost part of the sidewall turbulent boundary layers was exposed to a shock wave. The leading edge of the sidewall interaction reaches the lower wall first (ahead of the main shock induced separation). As shown by Wang *et al.* (2015), it reflects in the corner, but with only a small corner separation. The effect of the interaction with the lower surface was clarified by running a separate simulation with a slip-wall lower boundary condition. This showed that significant spanwise flow is developed irrespective of the lower boundary condition.

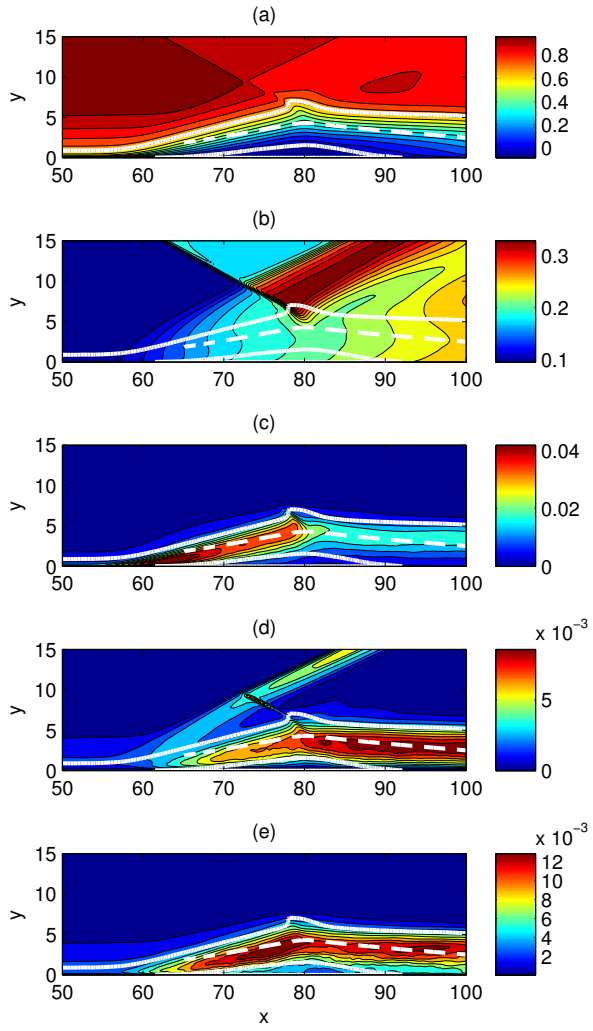

Figure 9. Mean flow and turbulent stresses in the interaction region: (a) velocity, (b) pressure (c) $\overline{u'^2}$, (d) $\overline{v'^2}$ (e) $\overline{w'^2}$. The upper white contour in each frame shows the sonic line and the lower contour shows $\overline{u} = 0$. The dashed line is a sample streamline.

In the present contribution we consider some more aspects of the WH2 case from Wang *et al.* (2015). Figure 9 shows contours on the centreline of the mean streamwise velocity (a), mean pressure (b) and the three normal components of the Reynolds stress (c-e). Also shown on each figure are three white lines corresponding from top to bottom to the sonic line (local $M = 1$, solid white line), a streamline located near the centre of the detached shear layer (dashed white line) and a line with zero mean streamwise velocity (solid white line), with reverse flow below this line. The shock pattern is best observed from figure 9(b) where the incoming shock crosses the compression waves caused by the boundary layer thickening, which starts upstream of the interaction. These reflected waves coalesce into a reflected shock. It can be seen how the incoming shock penetrates approximately to the sonic line and how the incoming shock is reflected as an expansion wave, with the shear-layer streamline then deflected downwards. This pattern is well known from previous studies and is representative of previous LES and experiments.

Figure 9(c-e) should in principle show the effect of turbulence in the outer part of the boundary layer passing through a shock wave that might be compared to previous work on normal-shock/turbulence interaction. However, on closer inspection that problem seems of little relevance here, since the changes in the turbulence are dominated by the shear layer. In figure 9(c) it is just possible to see a small increase in the magnitude of $\overline{u'^2}$ in the region above the sonic line. Instead, the streamwise Reynolds stress is dominated by the growth of turbulence in the detached shear layer, reaching a maximum at $x = 139$. Interestingly the peak shear stress doesn't exactly align with the streamline in these pictures.

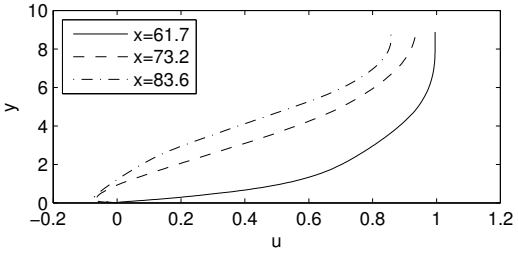

Figure 10. Velocity profiles at separation (solid line) and at two locations within the bubble.

Even more remarkable in figure 9(c) is the strong reduction in the streamwise components of the normal Reynolds stresses after the apex of the bubble. The stress decreases by a factor of approximately two between $x = 149$ and $x = 155$. Given that the local vorticity thickness is about 6, this reduction occurs within one vorticity thickness (and substantially less than one boundary layer 99% thickness). The explanation lies with what might be termed an indirect compressibility effect, based on the shear layer curvature near the apex of the bubble. For the streamline shown in figure 9 the minimum radius of curvature was determined to be 6.9. The direction of the curvature (opposite to the Görtler instability) is stabilizing and such a level of curvature, with the flow deflected by 15° within one vorticity thickness, is extreme. The curvature arises due to the reflection of the shock wave from the top of the bubble as an expansion, with subsequent flow turning only smeared over one boundary layer thickness. For a turbulence model to cope well with such a shock-induced separation, not only would it need to treat compressibility correctly, but also the stabilising effects of extremely strong curvature. In contrast to the behaviour of $\overline{u'^2}$ it can be seen that $\overline{v'^2}$ and $\overline{w'^2}$ are relatively unaffected by the sudden change of flow direction.

Figure 10 shows the velocity profile at separation and another two profiles through the separated flow, one upstream and one downstream of the bubble apex. For these two profiles the effective (convective) Mach number was estimated by taking the velocity difference between the external flow (under the shock waves) and the maximum reverse flow and the sound speed at the same two locations. This gave $M_c = 1.0$ for the upstream profile and $M_c = 0.9$ for the downstream profile (it may be noted that the freestream is slower at the second location due to the shock waves leading to the lower M_c). Based on the arguments of the previous section, these levels of M_c suggest significant compressibility effects on the turbulence. However the profiles are not well approximated by the hyperbolic tangents used in the previous section, and of course a wall is present here, so additional stability calculations are required to check the relevance of the previous results.

An impression of the instantaneous flow can be ob-

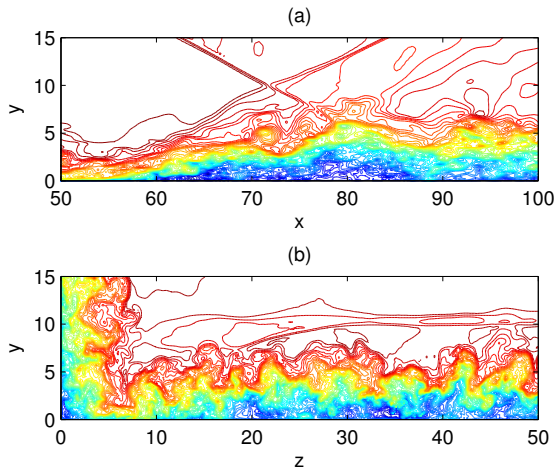

Figure 11. Contours of instantaneous streamwise velocity (a) in an $x-y$ plane at the centreline and (b) in a $y-z$ plane at $x = 73.2$.

tained from figure 11, which in part (a) shows an $x-y$ plane at the duct centreline and in part (b) shows a cut in a $y-z$ plane at $x = 73.2$. In figure 11(b) the sidewall boundary layer is visible and it can be seen that there is a significant penetration of high momentum fluid close to the wall, as also seen in Bermejo-Moreno *et al.* (2014), which is partly responsible for the mean flow to be attached in a region close to the sidewalls (cf. figure 8) and for the corner separation to be small. The horizontal contour lines present in the freestream are cuts through the impinging and reflected shock waves. In figure 11(a) it can be seen that the detached shear layer develops a wavy motion with a wavelength of perhaps 8-10 mm, while is figure 11(b) it can be seen that there are a series of undulations in the outer part of the boundary layer with a wavelength of approximately 6 mm. The resulting wave angles are around 60° which is not out of line with the $\theta - M_c$ diagram shown on figure 6(a), given that the local M_c is about one. More comparisons with stability theory are needed to confirm the potential role of inflectional instability in the generation of these structures.

CONCLUSIONS

The two main contributions of this paper are, firstly, a proposal to apply the stability map from the mixing layer to other flows in order to better understand the effect of Mach number. The stability map for the mixing layer shows how shear layer instability growth rates reduce with convective Mach number and how the variation of growth rate with wave angle also changes, leading to oblique modes being most unstable and also to a cut-off of modes with supersonic Mach number relative to the wave front. By considering compressibility effects to enter mainly at large scale, this shows how large scale structures and hence turbulence production can be modified by compressibility. Effective convective Mach numbers have been defined for turbulent spots and for boundary layers under pressure gradients to show how significant compressibility effects may be present in equilibrium boundary layers under adverse pressure gradient conditions.

Secondly, we have considered the development of the mean flow and Reynolds stresses in a 3D SWBLI problem with side wall effects included in the simulation. The high convective Mach numbers within the bubble suggest strong compressibility effects on the turbulence. The shock impinges near the apex of the bubble and is reflected as an expansion wave. The associated turning of the flow was shown to have a strong stabilising effect, leading to a reduction in turbulence intensity by over a factor of two. This is an example of an indirect compressibility effect, where the turbulence is governed by streamline curvature, which exists only due to the shock impingement.

Acknowledgements

The author would like to thank Bo Wang and Satya Jammy for providing databases for the 3D SWBLI case.

REFERENCES

Babinsky, H. & Harvey, J. 2011 *Shock Wave-Boundary-Layer Interactions*. Cambridge.

Bermejo-Moreno, I., Campo, L., Larsson, J., Bodart, J., Helmer, D. & Eaton, J.K. 2014 Confinement effects in shock wave/turbulent boundary layer interactions through wall-modelled large-eddy simulations. *J. Fluid Mech.* **758**.

Birch, S. F. & Eggers, J. M. 1973 A critical review of the experimental data for developed free turbulent shear layers. *Tech. Rep.* 32. NASA-SP.

Bradshaw, P. 1977 Compressible turbulent shear layers. *Ann. Rev. Fluid Mech.* **9**, 33–54.

Brown, G.L. & Roshko, A. 1974 Density effects and large structure in turbulent mixing layers. *J. Fluid Mech.* **64**, 775–816.

Chu, B.-T. & Kovásznay, S. G. 1958 Non-linear interactions in a viscous heat-conducting compressible gas. *Journal of Fluid Mechanics* **3**, 515–522.

Clemens, N.T. & Narayanaswamy, V. 2014 Low frequency unsteadiness of shock wave/turbulent boundary layer interactions. *Ann. Rev. Fluid Mech.* **46**, 469–492.

Coleman, G.N., Kim, J. & Moser, R.D. 1995 A numerical study of turbulent supersonic isothermal-wall channel flow. *J. Fluid Mech.* **305**, 159–183.

Doerffer, P., Hirsch, C., Dussauge, J.-P., Babinsky, H. & Barakos, G.N. 2010 *Unsteady Effect of Shock Wave Induced Separation*, *Notes on Numerical Fluid Mechanics and Multidisciplinary Design*, vol. 114. Springer.

Dolling, D. S. 2001 Fifty years of shock-wave/boundary-layer interaction research: What next? *AIAA Journal* **39** (8), 1517–1531.

Duan, L. & Martin, M. P. 2011 Direct numerical simulation of hypersonic turbulent boundary layers. Part 4. Effect of high enthalpy. *J. Fluid Mech.* **684**, 25–59.

Dupont, P., Haddad, C. & Debiève, J.F. 2006 Space and time organization in a shock-induced separated boundary layer. *J. Fluid Mech.* **559**, 255–277.

Fischer, M.C. 1972 Spreading of a turbulent disturbance. *AIAA Journal* **10**, 957–959.

Gad-El-Hak, M., Blackwelder, R.F. & Riley, J.J. 1981 On the growth of turbulent regions in laminar boundary-layers. *J. Fluid Mech.* **110**, 73–95.

Ganapathisubramani, B., Clemens, N.T. & Dolling, D.S. 2007 Effects of upstream boundary layer on the unsteadiness of shock-induced separation. *J. Fluid Mech.* **585**, 369–394.

Garneir, E., Adams, N.A. & Sagaut, P. 2009 *Large Eddy Simulation for Compressible Flows*. Springer.

Garnier, E. 2009 Stimulated detached eddy simulation of three-dimensional shock/boundary layer interaction. *Shock Waves* **19** (6), 479–486.

Garnier, E., Sagaut, P. & Deville, M. 2002 Large eddy simulation of shock/boundary-layer interaction. *AIAA Journal* **40** (10), 1935–1944.

Gaster, M., Kit, E. & Wygnanski, I. 1985 Large-scale structures in a forced turbulent mixing layer. *J. Fluid Mech.* **150**, 23–39.

Gatski, T.B. & Bonnet, J.P. 2009 *Compressibility, Turbulence and High-Speed Flow*.

Huang, P.G., Coleman, G.N. & Bradshaw, P. 1995 Compressible turbulent channel flows: DNS results and modelling. *J. Fluid Mech.* **305**, 185–218.

Jocksch, A. & Kleiser, L. 2008 Growth of turbulent spots in high-speed boundary layers on a flat plate. *Int. J. Heat and Fluid Flow* **29** (6), 1543–1557.

Krishnan, L. & Sandham, N. D. 2006 Effect of Mach number on the structure of turbulent spots. *J. Fluid Mech.* **566**, 225–234.

Larsson, J., Bermejo-Moreno, I. & Lele, S. K. 2013 Reynolds- and Mach-number effects in canonical shock-turbulence interaction. *J. Fluid Mech.* **717**, 293–321.

Lawal, A.A. 2002 Direct numerical simulation of transonic shock/boundary-layer interactions. PhD thesis, University of Southampton, Southampton, U.K.

Maeder, T., Adams, N.A. & Kleiser, L.. 2001 Direct simulation of turbulent supersonic boundary layers by an extended temporal approach. *J. Fluid Mech.* **429**.

Mahesh, K., Lele, S.K. & Moin, P. 1997 The influence of entropy fluctuations on the interaction of turbulence with a shock wave. *J. Fluid Mech.* **334**, 353–379.

Monkewitz, P.A. & Huerre, P. 1982 Influence of the velocity ratio on the spatial instability of mixing layers. *Phys. Fluids* **25** (7), 1137–1143.

Morris, P.J., Giridharan, M.G. & Lilley, G.M. 1990 On the turbulent mixing of compressible free shear layers. *Proc. Roy. Soc.-Mathematical and Phys. Sciences* **431** (1882), 219–243.

Pagella, A., Babucke, A. & Rist, U. 2004 Two-dimensional numerical investigations of small-amplitude disturbances in a boundary layer at Ma=4.8: Compression corner versus impinging shock wave. *Phys. Fluids* **16** (7), 2272–2281.

Pantano, C. & Sarkar, S. 2002 A study of compressibility effects in the high-speed turbulent shear layer using direct simulation. *J. Fluid Mech.* **451**, 329–371.

Papamoschou, D. & Roshko, A. 1988 The compressible turbulent shear-layer - an experimental-study. *J. Fluid Mech.* **197**, 453–477.

Piponniau, S., Dussauge, J.P., Debiève, J.F. & Dupont, P. 2009 A simple model for low-frequency unsteadiness in shock-induced separation. *J. Fluid Mech.* **629**, 87–108.

Pirozzoli, S. & Grasso, F. 2006 Direct numerical simulation of impinging shock wave/turbulent boundary layer interaction at m=2.25. *Phys. Fluids* **18** (6).

Plotkin, K.J. 1975 Shock-wave oscillation driven by turbulent boundary-layer fluctuations. *AIAA Journal* **13** (8), 1036–1040.

Ragab, S.A. & Wu, J.L. 1989 Linear instabilities in two-dimensional compressible mixing layers. *Physics of Fluids A-Fluid Dynamics* **1** (6), 957–966.

Redford, J. A., Sandham, N. D. & Roberts, G. T. 2012 Numerical simulations of turbulent spots in supersonic boundary layers: Effects of Mach number and wall temperature. *Progress in Aerospace Sciences* **52** (SI), 67–79.

Robinet, J.-Ch. 2007 Bifurcations in shock-wave/laminar-boundary-layer interaction: global instability approach. *J. Fluid Mech.* **579**, 85–112.

Sandham, N.D. & Reynolds, W.C. 1990 Compressible mixing layer - linear-theory and direct simulation. *AIAA Journal* **28** (4), 618–624.

Sandham, N.D. & Reynolds, W.C. 1991 3-dimensional simulations of large eddies in the compressible mixing layer. *J. Fluid Mech.* **224**, 133–158.

Sandham, N.D. & Sandberg, R.D. 2009 Direct numerical simulation of the early development of a turbulent mixing layer downstream of a splitter plate. *Journal of Turbulence* **10** (1), 1–17.

Sansica, A., Sandham, N.D. & Hu, Z. 2014 Forced response of a laminar shock-induced separation bubble. *Phy. Fluids* **26**, 957–959.

Sarkar, S. 1995 The stabilizing effect of compressibility in turbulent shear-flow. *J. Fluid Mech.* **282**, 163–186.

Sarkar, S., Erlebacher, G., Hussaini, M.Y. & Kreiss, H.O. 1991 The analysis and modeling of dilatational terms in compressible turbulence. *J. Fluid Mech.* **227**, 473–493.

Sartor, F. 2014 Unsteadiness in transonic shock-wave/boundary-layer interactions: experimental investigation and global stability analysis. PhD thesis, Aix-Marseille Université, France.

Slessor, M.D., Bond, C.L. & Dimotakis, P.E. 1998 Turbulent shear-layer mixing at high reynolds numbers: effects of inflow conditions. *J. Fluid Mech.* **376**, 115–138.

Smits, A.J. & Dussauge, J.-P. 2006 *Turbulent Shear Layers in Supersonic Flow*, 3rd edn. Springer.

Suzuki, T. & Colonius, T. 2006 Instability waves in a subsonic round jet detected using a near-field phased microphone array. *J. Fluid Mech.* **565**, 197–226.

Touber, E. 2010 Unsteadiness in shock-wave/boundary-layer interactions. PhD thesis, University of Southampton, Southampton, U.K.

Touber, E. & Sandham, N.D. 2009 Large-eddy simulation of low-frequency unsteadiness in a turbulent shock-induced separation bubble. *Theo. and Comp. Fluid Dyn.* **23** (2), 79–107.

Touber, E. & Sandham, N. D. 2011 Low-order stochastic modelling of low-frequency motions in reflected shock-wave/boundary-layer interactions. *J. Fluid Mech.* **671**, 417–465.

Vreman, A.W., Sandham, N.D. & Luo, K.H. 1996 Compressible mixing layer growth rate and turbulence characteristics. *J. Fluid Mech.* **320**, 235–258.

Vreman, B. 1995 Direct and large-eddy simulation of the compressible mixing layer. PhD thesis, University of Twente, Enschede, The Netherlands.

Wang, B., Sandham, N.D., Hu, Z. & Liu, W. 2015 Numerical study of oblique shock-wave/boundary-layer interaction considering sidewall effects. *J. Fluid Mech.* **767**, 526–561.

Wilcox, D.C. 2006 *Turbulence Modeling for CFD*, 3rd edn. McGraw-Hill.